*Progress In Electromagnetics Research C, Vol. 117, 173–184, 2021*

# Wideband Four-Port Compact Millimeter-Wave MIMO Antenna Configuration through Defected Ground Structure for Forthcoming 5G Handheld Devices

**Abdullah[1], Hamza Ahmad[1], MuhibUr Rahman[2, *], Muhammad Haris[1], and Muhammad Salman[1]**

**Abstract**—We presented a miniaturized defected ground structure-based millimeter-wave (MMW) contemporary MIMO antenna for 5G smart applications devices. The proposed MIMO antenna offers many advantages including high gain, compactness, planar geometry, wide impedance bandwidth, and reduced mutual coupling effects performance. The top layer of the proposed four-port MIMO antenna design comprises $1 \times 2$ rectangular patch array structures, with each placed at the middle of a $20 \times 20\,\text{mm}^2$ substrate of material (RO4350B) having thickness of 0.76 mm and loss tangent of 0.0037. For miniaturization and better performance, both the ground layer and radiating patches are defected with slots of a rectangular shape while an E-shaped slot is placed at the center of the ground plane. The operating impedance bandwidth of the proposed antenna ranges from 26.4 to 30.9 GHz incorporating the dominant portion of the mm-wave band. The proposed MIMO antenna is also characterized by the fundamental MIMO performance metrics such as Envelope Correlation Coefficient (ECC) which is less than 0.12 for any two-element array that encounters the mandatory standard of $< 0.5$, high Diversity gain (DG) reaching its ideal value of 10 as well as minimum isolation of $-19$ dB with a total efficiency of 85% at 28 GHz. These characteristics make the proposed compact four-port MIMO antenna one of the best candidates to be used in 5G portable devices.

## 1. INTRODUCTION

The foremost goal of the Internet of Things (IoT) is to flawlessly link new industries as well as new user experience with boosted functioning and reasonable prices with good efficiency [1]. The evolution of 5G (fifth generation) will introduce a route for very intelligent IoT technologies on a big scale [2]. The reason behind this latest achievement in the field of wireless technology is the 5G mobile communications evolution that leads the society to a stage of connectivity at an abundant rate and radio of significant capacity, having a reduced latency level. The 5G is expected to grab a maximum data rate of 20 Gbps alongside an improved networking capacity by introducing the latest portion of the spectrum known as the millimeter-wave (mm-wave) band from 30–300 GHz [3]. However, these millimeter-waves suffer from various constraints, comprising free-space loss, high atmospheric losses, and bigger manufactured cost [4]. Intriguingly, at 28 GHz with some other mm-wave bands, the propagation losses are very low as compared to others in this portion of the whole mm-wave spectrum [5]. The real-world execution of 5G systems is conditional on the efficient configuration of design analysis of the 5G antennas as these are the fundamental elements of all communication systems [6]. Furthermore, 5G mm-wave antennas are intended to have high efficiency and gain performance values as well as operate for larger bandwidths by improving SNR and data rate. Due to the many benefits of design simplicity and planar

*Received 18 November 2021, Accepted 22 December 2021, Scheduled 2 January 2022*
* Corresponding author: MuhibUr Rahman (muhibur.rahman@polymtl.ca).
[1] Department of Electrical Engineering, University of Engineering and Technology, Mardan, Pakistan. [2] Department of Electrical Engineering, Polytechnique Montreal, University of Montreal, Montreal, QC H3T1J4, Canada.

structure, considerable research has been dedicated to mm-wave wireless communications by utilizing printed antennas [7, 8]. Furthermore, these printed mm-wave antennas present the main feature of 5G technology to increase the capacity of the 5G network and reliability because these antennas simplify the MIMO configuration design with low structure complexity [9]. The reduction of size and mutual coupling in the MIMO antenna system are the key challenging factors to be considered while a MIMO antenna is designed for 5G Devices. By using decoupling structures such as defected ground structures, neutralization lines, and diversity techniques, significant improvement of isolation can be obtained [8]. Various researchers have reported MIMO antennas for 5G applications working at 28 GHz band ranging from 26 to 30 GHz [10–20]. A quad-element patch antenna through defected ground structure technique with MIMO layout is presented for high gain and wideband application in [13]. Similarly, [14] utilizes an H-shaped patch eight-element MIMO antenna for broad-band mm-wave 5G communication. Moreover, a dipole antenna is developed in [10] with an array metamaterial structure for obtaining high gain in the edge-fire direction. A patch antenna loaded with a superstrate is designed in [11] for increasing gain as well as the operating bandwidth. Due to the existence of a physical gap between the superstrate and the radiator, these kinds of antennas suffer from high profile and mechanical problems. Also, a microstrip patch antenna with dual-band operation at 28 and 38 GHz is developed and presented in [17]. Although a reasonable gain of 12.3 dBi is achieved at both desired operating frequency bands, it has a very narrow bandwidth of less than 1 GHz. An antenna based on EBG is designed in [18] which operates at mm-wave bandwidth of 0.8 GHz. To prevent conductor losses of metallic radiators, antennas having dielectric resonators are used in the design of mm-wave antennas as well [15, 16].

To accomplish the discussion, most of the antennas mentioned above are affected by the problem of either operating limited bandwidth portion or minimum isolation which makes them less suitable for broadband 5G mm-wave applications. Furthermore, large volumes and high-profile antennas are also not appropriate for incorporating into compact 5G handheld applications devices. After a comprehensive review of the outstanding works contributed for the same 5G mm-wave smart application devices, we can conclude that the design of a compact mm-wave antenna and its MIMO configuration having high isolation, wide operating mm-wave bandwidth, and high diversity gain with an uncomplicated geometry is quite challenging.

In this work, a compact 5G mm-wave antenna along with its four-element MIMO configuration is illustrated for 5G smart devices. The proposed four-port MIMO antenna is distinguished by ECC of reasonable value, wide operating bandwidth, high diversity gain performance, high isolation, and very compact size suitable for forthcoming 5G handheld devices.

The arrangement of this paper is in the following manner. Section 2 deals with antenna design including design of single element antenna, two element array antenna, and proposed MIMO antenna. Section 3 deals with simulated results in terms of reflection coefficients and parametric analysis for patch length and width. Section 4 gives the simulated and measured results of the proposed four port MIMO antenna. Section 5 provides the antenna performance in terms of ECC and diversity gain, followed by a conclusion section.

## 2. ANTENNA EVOLUTION AND THEORETICAL ANALYSIS

### 2.1. Design of Single Element Patch Antenna

At the first stage, a modified ordinary patch antenna of rectangular shape with a copper ground layer clothing of 0.0035 mm thickness is etched on the top side of substrate RO4350B material as shown in Figure 1. The relative permittivity, thickness, and loss tangent of this material used for this design are 3.66, 0.76 mm, and 0.0037, respectively. To obtain the operating frequency of 28 GHz, standard equations of rectangular patch antenna are used to design a reference antenna as [19]:

$$W_p = \frac{C_o}{2f_c}\sqrt{\frac{2}{\varepsilon_r + 1}} \tag{1}$$

where $W_p$ represents the patch width, $C$ the speed of light, $f_c$ the central frequency, and $\gamma_r$ the relative permittivity of the utilized substrate. The length of the corresponding patch is given as:

$$L_p = \frac{C_o}{2f_c\sqrt{\varepsilon_{reff}}} \tag{2}$$

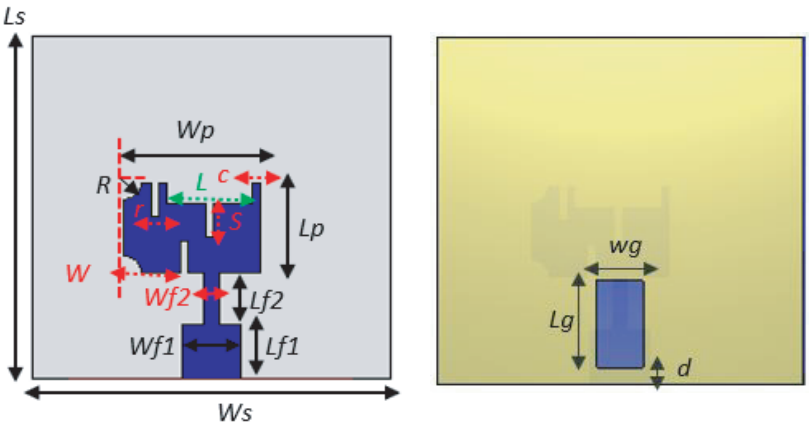


**Figure 1.** Layout of modified conventional rectangular patch antenna. (a) Front view. (b) Back view with defected ground structure. Optimized parameters for this case: $W_s = L_s = 10\,\text{mm}$, $W_p = 3.78\,\text{mm}$, $L_p = 2.64\,\text{mm}$, $w_{f1} = 1.6\,\text{mm}$, $L_{f1} = 1.6\,\text{mm}$, $L_{f2} = 1.5\,\text{mm}$, $w_{f2} = 0.42\,\text{mm}$, $L = 2.4\,\text{mm}$, $c = 0.2\,\text{mm}$, $S = 1\,\text{mm}$, $r = 0.2\,\text{mm}$, $R = 0.5\,\text{mm}$, $w = w_g = 1.25\,\text{mm}$, $L_g = 2.5\,\text{mm}$, $d = 0.5\,\text{mm}$.

where $L_p$ represents the patch length, and $\gamma_{reff}$ is the effective relative permittivity of the substrate which can be calculated as [20]:

$$\varepsilon_{reff} = \frac{\varepsilon_r + 1}{2} + \frac{\varepsilon_r - 1}{2}\left(1 + \frac{12h}{w_f}\right)^{-0.5} \tag{3}$$

Eqs. (1)–(3) are used to calculate the length and width of the corresponding patch antenna termed as the reference antenna. This reference antenna is too bulky, and we have utilized a defected ground structure to properly utilize the electrical length of the proposed structure. This is the main reason that DGS structures have considerably reduced the antenna size in comparison to the basic equations of the patch antenna discussed in Eqs. (1)–(3).

Initially, the modified patch antenna with slots of different dimensions is simulated which has a narrow operating bandwidth consisting of two parts. At the second stage, a rectangular slot is etched at the backside of the main feedline from the ground layer which changes the effective inductance and capacitance of the whole patch antenna with an increase in bandwidth. This two-element array was used later in a four-port MIMO configuration with a substrate dimension of $20 \times 20 \times 0.76\,\text{mm}^3$.

### 2.2. Design of Two Element Array Antenna

The second stage includes the design of a dual-element array with a balanced feeding network having the same modified rectangular patch to obtain the wideband operation as well as high gain performance as shown in Figure 2. This two-element array is then simulated with and without a defected ground structure. It is found that the antenna now operates for larger bandwidth and enhanced reflection coefficient for 28 GHz frequency in comparison to single element antenna. This is because DGS enhances the electrical length of the antenna which in turn increases the impedance bandwidth.

## 3. SIMULATION AND PARAMETRIC ANALYSIS

CST Microwave Studio Suite was used to perform the numerical analysis from single element antenna to 4-port MIMO configuration. Different antenna performance parameters such as reflection and transmission coefficients, gain, efficiency, and radiation pattern have competed for all cases in this section. In Figure 3, the simulated reflection coefficient graphs of single element patch antenna are depicted. It can be observed that the operating bandwidth, in this case, consists of two bands 27.1–28.7 GHz and 29.6–31.2 GHz with a maximum reflection coefficient of $-15\,\text{dB}$ and at 28 GHz. After

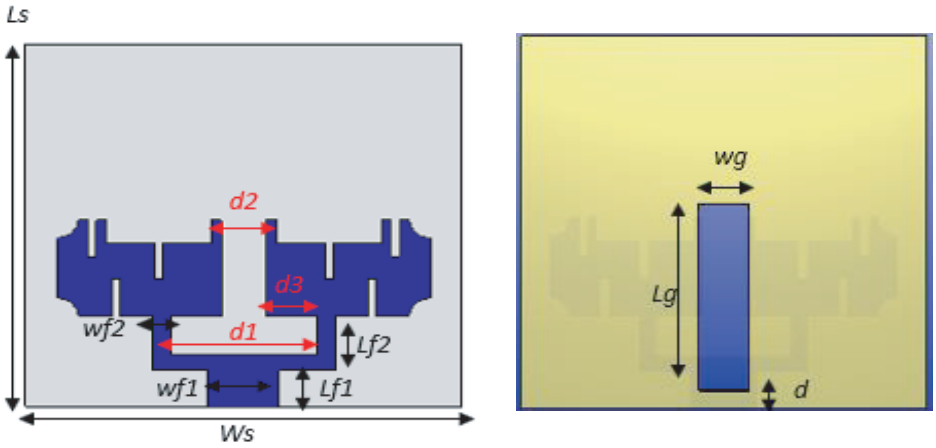


**Figure 2.** Configuration of two element array antenna. (a) Front view. (b) Back view with defected ground structure. Optimized parameters values: $W_s = L_s = 10\,\text{mm}$, $w_{f1} = 1.6\,\text{mm}$, $L_{f1} = 1\,\text{mm}$, $L_{f2} = 1.5\,\text{mm}$, $w_{f2} = 0.42\,\text{mm}$, $d_1 = 3.32\,\text{mm}$, $d_2 = 1\,\text{mm}$, $d_3 = 1.13\,\text{mm}$, $w_g = 1.25\,\text{mm}$, $L_g = 4.5\,\text{mm}$, $d = 0.5\,\text{mm}$.

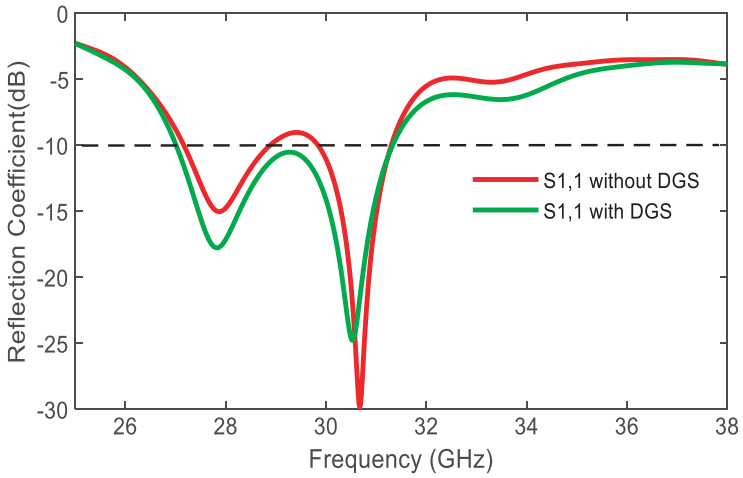


**Figure 3.** Simulated $S$-parameters comparison for the conventional modified rectangular patch antenna with and without defected ground structure.

simulation, the operating impedance bandwidth for the same modified patch antenna increases ranging from 27 to 31.3 GHz as a single portion with a maximum reflection coefficient of −18 dB and maximum gain of 6.8 dBi at 28 GHz frequency as illustrated in Figure 3. It also shows the simulated reflection coefficient of the modified single element rectangular patch antenna in both scenarios.

Figure 4 demonstrates the reflection coefficient of the simulated two element array antenna. The reflection coefficient is −32 dB with an operating bandwidth of 3.9 GHz (30.7–26.8) without DGS. When a DGS is inserted in the structure, −40 dB reflection coefficient is achieved with enhancement in bandwidth (4.2 GHz) and gain (7.3 dBi) at 28 GHz compared to the preceding single element patch antenna.

A defected ground structure of rectangular shape used in the antenna design process of this work is considered for attaining a smaller resonance without disturbing the size of the antenna. The consequences of this DGS on the reflection coefficient, resonating frequency, and bandwidth performance are described in this section. Figure 5(a) illustrates the reflection coefficient of the two-element array antenna for various values of $L_g$ (length of the slots etched from the ground plane). It can be observed

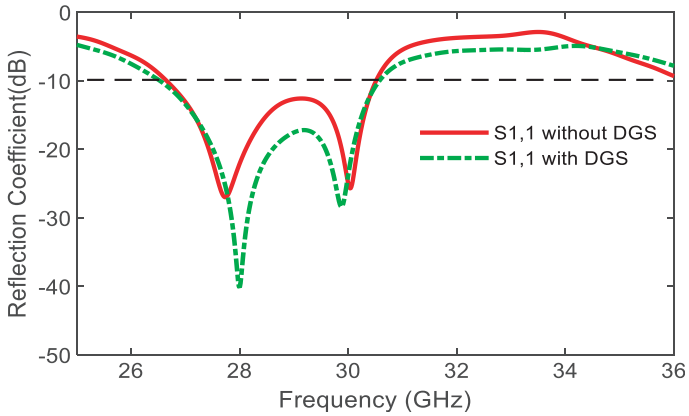


**Figure 4.** Simulated $S$-parameters comparison for the proposed two-element array antenna with and without defected ground structure.

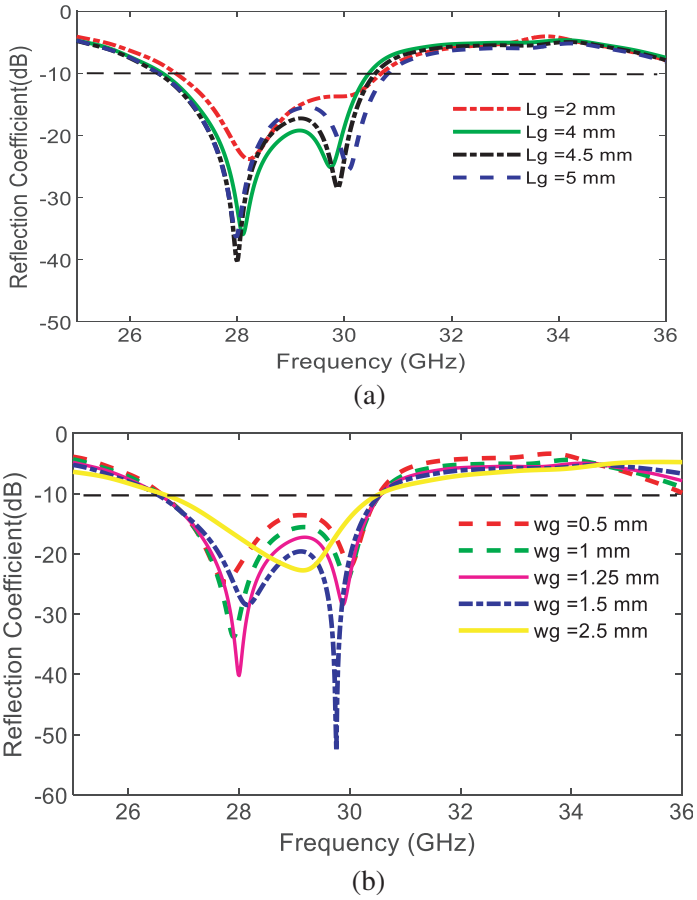


**Figure 5.** Parametric analysis of the reflection coefficient at different values for DGS in two-element array antenna. (a) Length, $L_g$; (b) Width, $W_g$.

that decreasing the value of $L_g$ causes a two-portion smaller bandwidth with minimum reflection coefficient than larger values 4.5–5 mm. Similarly, the effects of different $w_g$ values (width of the ground slot) are illustrated in Figure 5(b). It can be seen from Figure 5 that for $L_g = 4.5$ mm and $w_g = 1.25$ mm, a maximum reflection coefficient of $-40$ dB is achieved for 28 GHz frequency with a wideband characteristic.

## 4. FOUR-PORT MIMO ANTENNA

In this section, we demonstrate a proposed four port MIMO antenna. In the previous section, we designed a two-element array antenna, and following the same concept, we extended it to a four-port MIMO antenna configuration shown in Figure 6. The overall size of the proposed four-port MIMO antenna is $20 \times 20 \times 0.76\,\text{mm}^3$ with four rectangular shape DGSs at the backside of each feedline and an E-shaped DGS at the midpoint having equal distance from previously presented DGS of the ground plane to reduce the mutual coupling effects. Each two-element array antenna used is placed at the middle position of the substrate material exhibiting good MIMO performances for this positioning. The simulated reflection coefficient of the MIMO antenna is shown in Figure 7.

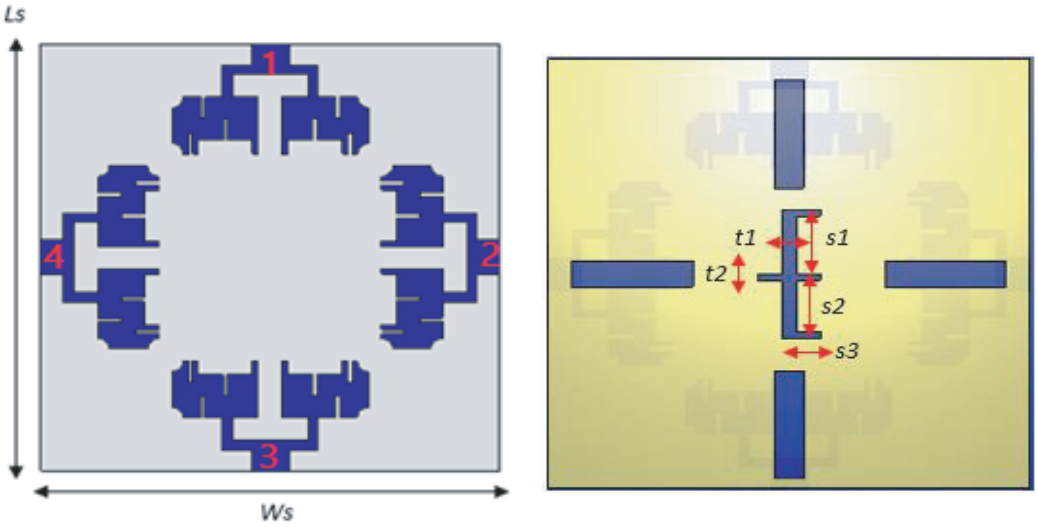


**Figure 6.** Geometrical configuration of the proposed four port MIMO antenna based on DGS. (a) Front view; (b) Back view.

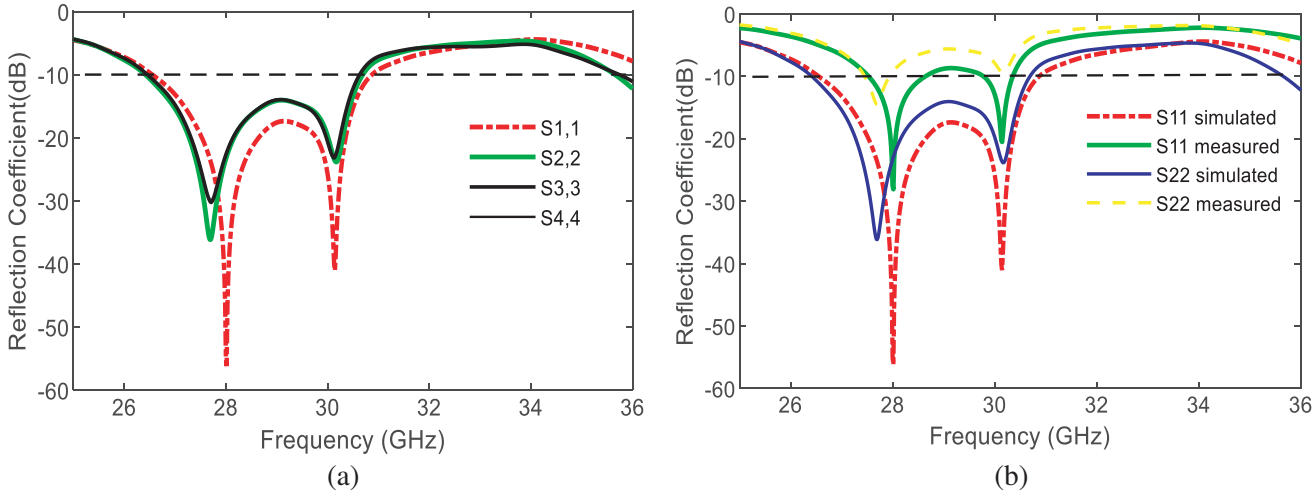


**Figure 7.** (a) Simulated Reflection coefficient of 4-Port MIMO Antenna system with DGS. (b) MIMO Antenna system's Reflection Coefficient evaluation of simulated and calculated results.

## 5. RESULTS AND DISCUSSION OF MIMO ANTENNA

### 5.1. S-Parameter Analysis of MIMO Configuration

This section deals with the analysis of the $S$-parameter analysis. Figure 8 shows the analysis of reflection coefficients ($S_{11}$, $S_{22}$, $S_{33}$, $S_{44}$) while Figure 9 shows transmission coefficients ($S_{11}$, $S_{22}$, $S_{33}$, $S_{44}$) for the four-port MIMO configuration based on the same single-port two-element array antenna as a building block discussed in the previous section. The operating bandwidth curve of the 4-port ($4 \times 4$) MIMO antenna configuration ranges from 26.4 to 30.9 GHz. The impedance bandwidth achieved is 4.9 GHz with the highest gain of 9.6 dBi at 28 GHz frequency while maximum reflection coefficient ($S_{11}$) is equal to $-55$ dB. The surface current distribution of the proposed antenna is also provided in Figure 8 for more clarity. Figure 9 shows the transmission coefficient curve for a 4-port MIMO antenna system. It is observed from the transmission coefficient curve that there is the lowest isolation of $-19$ dB between Ant1 and Ant3, and a similar behavior is observed between Ant4 and Ant1. In addition, good isolation is attained for the other antenna pairs 1 and 2, 3 and 4, 4 and 2, 1 and 3. An E-shaped defected ground structure (DGS) is integrated at the ground layer of the 4-port MIMO antenna system to further decrease the effects of mutual coupling.

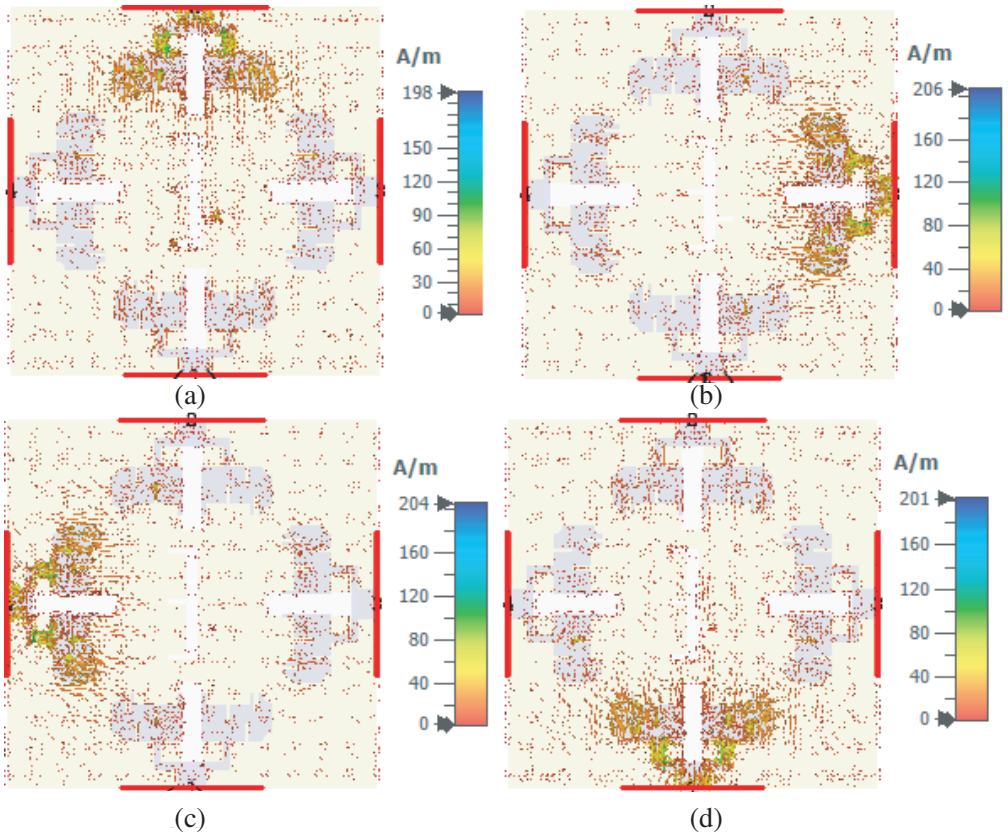


**Figure 8.** Surface current distributions of the proposed antenna at 28 GHz. (a) Antenna 1 is excited; (b) Antenna 2 is excited; (c) Antenna 3 is excited; (d) Antenna 4 is excited.

### 5.2. MIMO Performance Parameters

The performance of a MIMO antenna system can be determined from MIMO performance metrics such as Envelope Correlation Coefficient (ECC) and Diversity Gain (DG) discussed below.

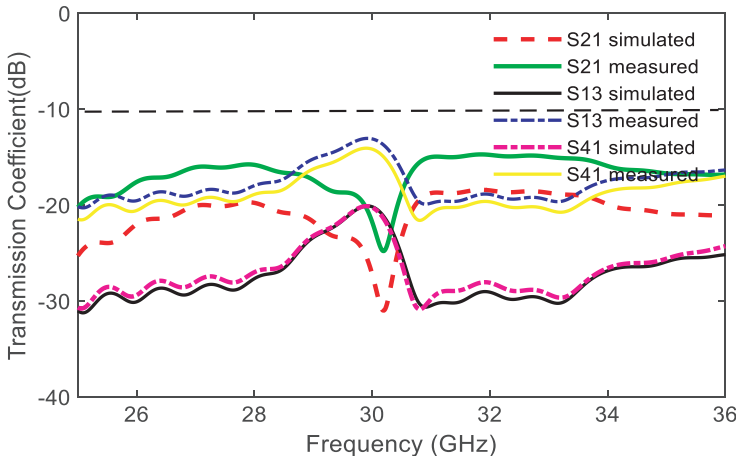


**Figure 9.** MIMO Antenna system's Transmission Coefficient evaluation of simulated and calculated results.

### *5.2.1. Envelope Correlation Coefficient (ECC)*

ECC shows the mutual coupling effects, and the lower the value of ECC is, the lower the mutual coupling will be (good ports isolation). Figure 10 shows the ECC curve in which its value for the proposed MIMO antenna system is nearly equal to 0.0012 ($< 0.5$, standard value) for the operating 26.4–30.9 GHz bandwidth. The equation utilized for the calculation of ECC is given as [21]:

$$\rho_{eij} = \frac{\left|S_{ii}^{*}S_{ij} + S_{ji}^{*}S_{jj}\right|^{2}}{\left(1 - |S_{ii}|^{2} - S_{ij}^{2}\right)\left(1 - |S_{ji}|^{2} - S_{jj}^{2}\right)} \tag{4}$$

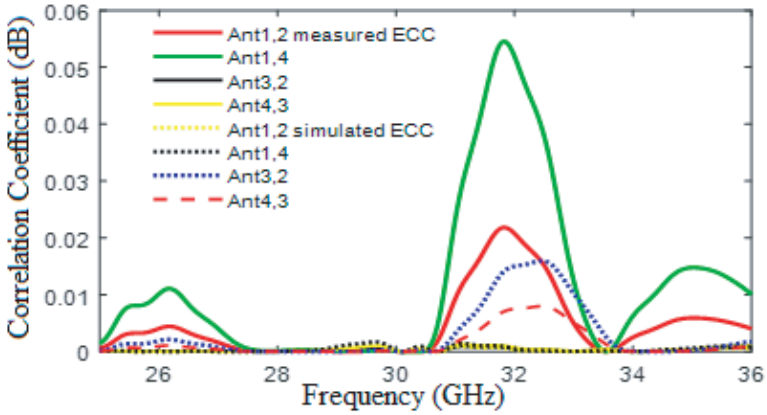


**Figure 10.** Simulated and calculated ECC curve of the proposed MIMO system.

### *5.2.2. Diversity Gain (DG)*

The decrease in transmission power after diversity schemes are applied is shown by diversity gain (DG). The DG curve for the planned MIMO antenna system is shown in Figure 11 in which the DG value obtained is nearly equal to 9.4 dB for Ant1 and Ant2, Ant2 and Ant3, and other pairs in the operating bandwidth. The diversity gain is calculated based on the equation as [22]:

$$DG = 10\sqrt{1 - |P_{eij}|^{2}} \tag{5}$$

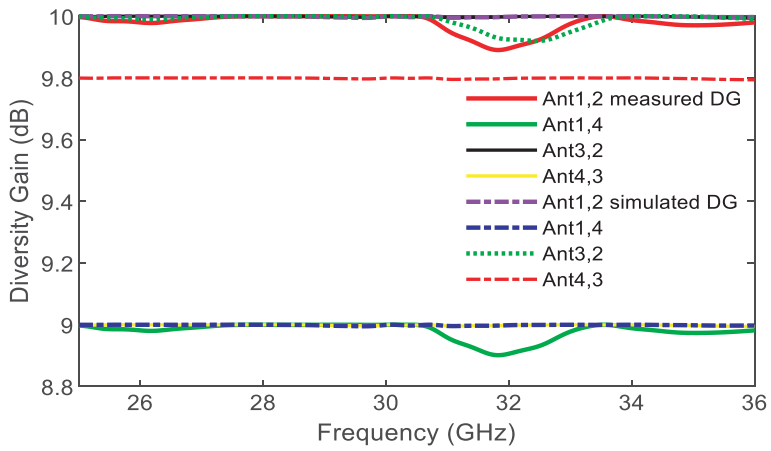


**Figure 11.** Simulated and measured DG curve of the proposed MIMO antenna.

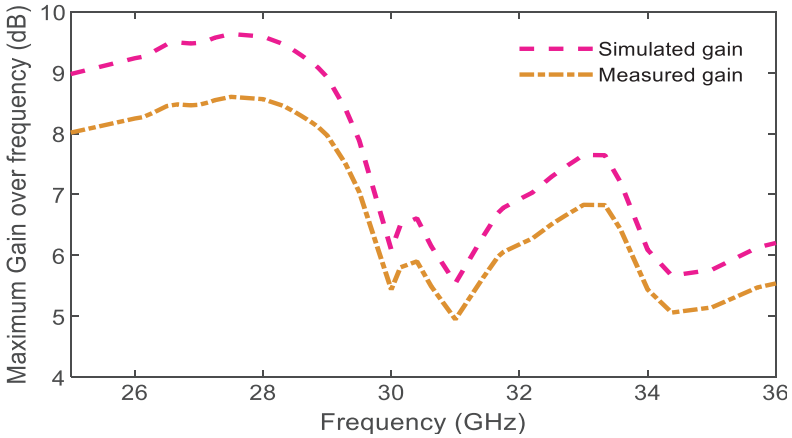


**Figure 12.** Simulated and measured maximum gain over the frequency curve of the planned MIMO antenna.

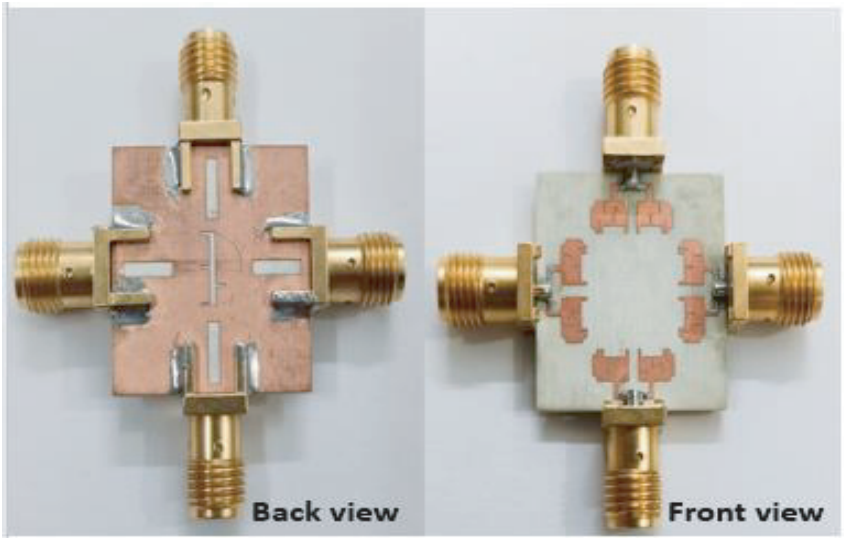


**Figure 13.** Fabricated prototype of the proposed MIMO antenna.

The measurement arrangement using a network analyzer and far-field anechoic chamber of the proposed MIMO antenna is shown in Figures 14(a) and (b). The simulated and measured radiation patterns of the proposed antenna taken at $YZ$ and $XZ$ planes are shown in Figures 15(a) and (b), respectively. The proposed antenna exhibits overall good performance for both simulated and measured radiation performances.

## 6. COMPARISON WITH RECENT STATE OF THE ART ANTENNAS

The corresponding simulated gain at a desired frequency band is shown in Figure 12 which is also correlated with the measured response. Also, the fabricated prototype of the proposed antenna is shown in Figure 13. The comparison of the proposed antenna with recent state of the art is tabulated in the form of Table 1. The proposed antenna is superior to the recent state of the arts in terms of bandwidth, gain, ECC, DG, and more specifically the size.

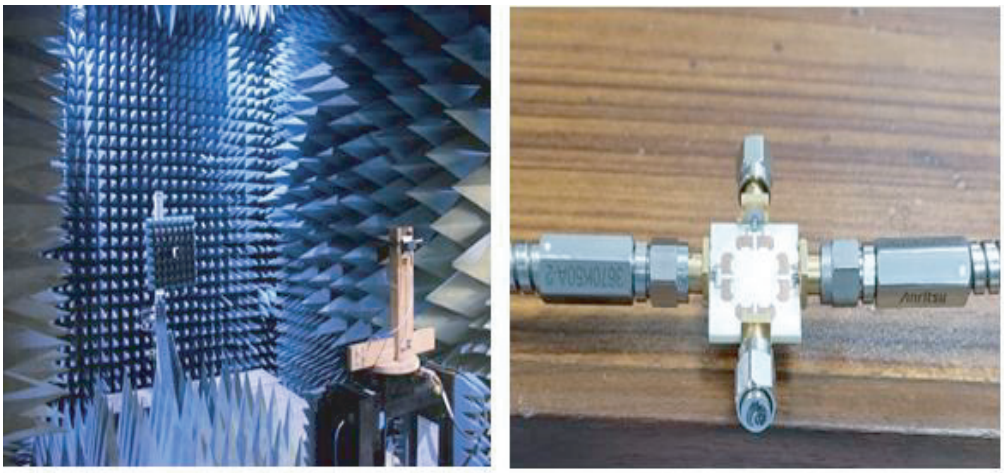


**Figure 14.** Snapshots taken during measurement; (a) Radiation pattern measurement; (b) $S$-parameters measurement.

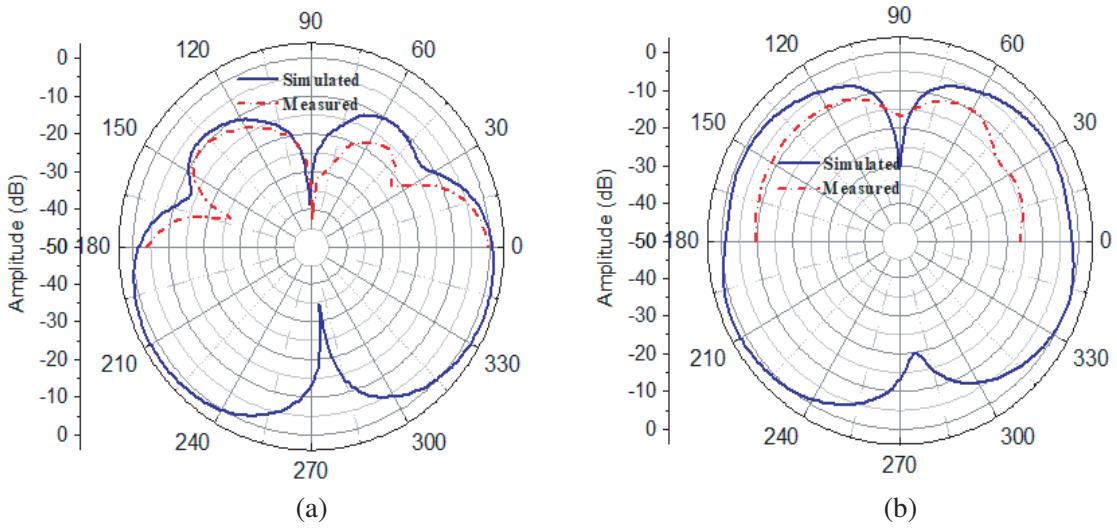


**Figure 15.** Radiation pattern of the proposed antenna at 28 GHz; (a) Simulated vs. Measured at $YZ$-plane; (b) Simulated vs. Measured at $XZ$-plane.

**Table 1.** Comparison with recent state of the art antennas (N/A means not applicable).

| Ref. | Freq. (GHz) | Size | No. of Ports | Bandwidth (GHz) | Gain (dB/dBi) | ECC | DG (dB) |
|---|---|---|---|---|---|---|---|
| [12] | 28 | $30 \times 35 \times 0.76\,\text{mm}^3$ | Four | 4.1 | 8.4 dBi | $< 0.01$ | $> 9.91$ |
| [23] | 28 | $19 \times 19 \times 7.608\,\text{mm}^3$ | Four | 8.1 | 14.2 dBi | N/A | N/A |
| [24] | 28 | $20 \times 20 \times 0.25\,\text{mm}^3$ | Two | 0.87 | 8 dBi | 0.11 | 9.9 |
| [25] | 28 | $68 \times 130 \times 0.50\,\text{mm}^3$ | Four | 1.0 | 12 dBi | N/A | N/A |
| [26] | 24 | $15 \times 19 \times 0.25\,\text{mm}^3$ | Two | 0.8 | 6.1 dBi | 0.23 | 9.7 |
| This work | 28 | $20 \times 20 \times 0.76\,\text{mm}^3$ | Four | 4.9 | 9.6 dBi | 0.23 | 9.4 |

## 7. CONCLUSION

In this work, we present a compact size 4-port MIMO antenna with defective ground structures for 5G mm-wave applications. Each port is composed of a $1 \times 2$ antenna array arrangement having an equaling parallel branch feeding network. Defected ground structures of rectangular and E shapes are used to enhance the MIMO performance as well as to reduce mutual coupling effects in $20 \times 20\,\text{mm}^2$ compact dimensions. The operating frequency band for the proposed MIMO system ranges from 26.4.0 to 30.9 GHz having a bandwidth of 3.47 and retaining a maximum gain of 9.6 dBi at 28 GHz. Similarly, the MIMO performance analyses of ECC and DG were also computed and found to be inside an essentially standard range. The miniaturized size of the proposed radiator will make it the best candidate to be used for inevitable 5G mm-wave applications.

## REFERENCES

1. Yao, M., M. M. Sohul, X. Ma, V. Marojevic, and J. H. Reed, "Sustainable green networking: Exploiting degrees of freedom towards energy-efficient 5G systems," *Wireless Netw.*, Vol. 25, No. 3, 951–960, 2019.
2. Rappaport, T. S., S. Sun, R. Mayzus, H. Zhao, Y. Azar, K. Wang, et al., "Millimeter wave mobile communications for 5G cellular: It will work!," *IEEE Access*, Vol. 1, 335–349, 2013.
3. Yilmaz, T. and O. B. Akan, "On the use of low terahertz band for 5G indoor mobile networks," *Comput. Electr. Eng.*, Vol. 48, 164–173, 2015.
4. Rahman, M., M. Naghshvarian Jahromi, S. S. Mirjavadi, and A. M. Hamouda, "Bandwidth enhancement and frequency scanning array antenna using novel UWB filter integration technique for OFDM UWB radar applications in wireless vital signs monitoring," *Sensors*, Vol. 18, 3155, 2018.
5. Roh, W., J. Y. Seol, J. Park, B. Lee, J. Lee, Y. Kim, et al., "Millimeter-wave beamforming as an enabling technology for 5G cellular communications: Theoretical feasibility and prototype results," *IEEE Comm. Mag.*, Vol. 52, No. 2, 106–113, 2014.
6. Khan, T., M. Rahman, A. Akram, Y. Amin, and H. Tenhunen, "A low-cost CPW-fed multiband frequency reconfigurable antenna for wireless applications," *Electronics*, Vol. 8, 900, 2019.
7. Kumar, M. N. and T. Shanmuganantham, "Division shaped substrate integrated waveguide slot antenna for millimeter wireless/automotive radar applications," *Comput. Electr. Eng.*, Vol. 71, 667–675, 2018.
8. Naqvi, A. H., J. H. Park, C. W. Baek, and S. Lim, "V-band end-fire radiating planar micromachined helical antenna using Through-Glass Silicon Via (TGSV) technology," *IEEE Access*, Vol. 26, No. 7, 87907–87915, Jun. 2019.

9. Saad, A. A. and H. A. Mohamed, "Printed millimeter-wave MIMO-based slot antenna arrays for 5G networks," *AEU — Int. J. Electron. Commun.*, Vol. 99, 59–69, 2019.
10. Wani, Z., M. P. Abegaonkar, and S. K. Koul, "A 28-GHz antenna for 5G MIMO applications," *Progress In Electromagnetics Research*, Vol. 78, 73–79, 2018.
11. Hussain, N., M. J. Jeong, J. Park, and N. Kim, "A broadband circularly polarized Fabry-Perot resonant antenna using a single-layered PRS for 5G MIMO applications," *IEEE Access*, Vol. 7, 42897–42907, 2019.
12. Khalid, M., S. Iffat Naqvi, N. Hussain, M. Rahman, S. S. Mirjavadi, M. J. Khan, et al., "4-port MIMO antenna with defected ground structure for 5G millimeter wave applications," *Electronics*, Vol. 9, No. 1, 71, 2020.
13. Jilani, S. F. and A. Alomainy, "Millimetre-wave T-shaped MIMO antenna with defected ground structures for 5G cellular networks," *IET Microw. Antennas Propag.*, Vol. 12, No. 5, 672–677, 2018.
14. Tu, D. T. T., N. T. B. Phuong, P. D. Son, and V. Van Yem, "Improving characteristics of 28/38 GHz MIMO antenna for 5G applications by using double-side EBG structure," *J. Commun.*, Vol. 14, No. 1, 1–8, 2019.
15. Rahman, M., A. Haider, and M. Naghshvarianjahromi, "A systematic methodology for the time-domain ringing reduction in UWB band-notched antennas," *IEEE Antennas and Wireless Propagation Letters*, Vol. 19, No. 3, 482–486, Mar. 2020.
16. Zhang, Y., J. Y. Deng, M. J. Li, D. Sun, and L. X. Guo, "A MIMO dielectric resonator antenna with improved isolation for 5G mm-wave applications," *IEEE Antennas Wirel. Propag. Lett.*, Vol. 18, No. 4, 747–751, 2019.
17. Khan, T. and M. Rahman, "Design of low-profile frequency reconfigurable antenna for multiband applications," *International Journal of Electronics Letters*, 1–18, 2020.
18. Parvathi, K. S. and S. R. Gupta, "Novel dual-band EBG structure to reduce mutual coupling of air gap based MIMO antenna for 5G application," *AEU — International Journal of Electronics and Communications*, Vol. 138, 153902, 2021.
19. Rahman, M., D.-S. Ko, and J.-D. Park, "A compact multiple notched ultra-wide band antenna with an analysis of the CSRR-TO-CSRR coupling for portable UWB applications," *Sensors*, Vol. 17, 2174, 2017.
20. Rahman, M., M. Nagshvarian Jahromi, S. S. Mirjavadi, and A. M. Hamouda, "Compact UWB band-notched antenna with integrated bluetooth for personal wireless communication and UWB applications," *Electronics*, Vol. 8, 158, 2019.
21. Park, J., M. Rahman, and H. N. Chen, "Isolation enhancement of wide-band MIMO array antennas utilizing resistive loading," *IEEE Access*, Vol. 7, 81020–81026, 2019.
22. Iffat Naqvi, S., N. Hussain, A. Iqbal, M. Rahman, M. Forsat, S. S. Mirjavadi, and Y. Amin, "Integrated LTE and millimeter-wave 5G MIMO antenna system for 4G/5G wireless terminals," *Sensors*, Vol. 20, 3926, 2020.
23. Hussain, N., M. Jeong, J. Park, and N. Kim, "A broadband circularly polarized Fabry-Perot resonant antenna using a single-layered PRS for 5G MIMO applications," *IEEE Access*, Vol. 7, 42897–42907, 2019.
24. Zhang, Y., J. Deng, M. Li, D. Sun, and L. Guo, "A MIMO dielectric resonator antenna with improved isolation for 5G mm-wave applications," *IEEE Antennas and Wireless Propagation Letters*, Vol. 18, No. 4, 747–751, 2019.
25. Ikram, M., Y. Wang, M. S. Sharawi, and A. Abbosh, "A novel connected PIFA array with MIMO configuration for 5G mobile applications," *2018 Australian Microwave Symposium (AMS)*, 19–20, Brisbane, QLD, 2018.
26. Iqbal, A., et al., "Electromagnetic bandgap backed millimeter-wave MIMO antenna for wearable applications," *IEEE Access*, Vol. 7, 111135–111144, 2019.